Electrorheological Characteristics of Solvent-Cast Polypyrrole/Clay Nanocomposite

D. P. Park,[1] S. T. Lim,[1] J. Y. Lim,[1] H. J. Choi,[1] S. B. Choi[2]

[1]*Department of Polymer Science and Engineering, Inha University, Incheon 402751, Korea*
[2]*Department of Mechanical Engineering, Inha University, Incheon 402751, Korea*

Received 4 February 2008; accepted 21 July 2008
DOI 10.1002/app.29636
Published online 5 February 2009 in Wiley InterScience (www.interscience.wiley.com).

ABSTRACT: A solvent-casting method was applied to prepare intercalated polypyrrole (PPy)/organoclay nanocomposite for its electrorheological (ER) application under an applied electric field when dispersed in silicone oil. Soluble PPy was synthesized using sodium di(2-ethylhexyl) sulfosuccinate (NaDEHS) as a doping agent at first, and its chemical structure and thermal property were examined using NMR and TGA, respectively. Insertion of the soluble PPy chain into an interlayer of the organoclay was confirmed by a X-ray diffraction and its morphology was also examined by both SEM and TEM. Its ER property was examined under an applied electric field, regarding flow curve and universal yield stress. © 2009 Wiley Periodicals, Inc. J Appl Polym Sci 112: 1365–1371, 2009

Key words: soluble polypyrrole; nanocomposite; electrorheological fluid

INTRODUCTION

Electrorheological (ER) fluids, typically composed of micron-sized conducting or semiconducting particles dispersed in a nonconducting medium oil, produce dramatic, reversible response in rheological properties of a suspension when applied to an electric field normal to the flow direction.[1–3] The dipole–dipole interactions among the particles lead to fibril structures via a chain formation and alignment of particles along the applied electric field direction with strings of particle orientation.[4–6] These fibrillar particle structures result in the dielectric constant mismatch between the particles and the insulating oil. As a result, these colloidal suspensions under a high electric field strength and relatively high particle concentration exhibit strong resistance against a shear deformation. These ER fluids, along with their magnetic analogs, magnetorheological fluids,[7] can be classified into anhydrous- or wet-based systems according to both ER mechanism and the presence of water. Overcoming the disadvantages of wet-based ER materials[8] of water evaporation, device corrosion, and limited operation temperature range, dry-based ER systems such as semiconducting polymers,[9,10] modified biopolymers,[11–13] and organic/inorganic hybrid systems[14–16] have been extensively investigated. Anhydrous ER systems were more generally adopted because of their chemical and physical stabilities rather than wet-based system. As one of the novel conducting polymers, polypyrrole (PPy) has also been introduced as an ER material.[17] Insolubility of the PPy in general organic solvents even helps its applicability into the ER fields.

PPy is a well-known conducting polymer because of its good thermal and environmental stability as well as its superior conductivity.[18] However, PPy is known to be insoluble in common organic solvents in general because of its strong inter and intramolecular interaction and crosslinking. Meanwhile, poly (3-substituted pyrrole) such as poly(3-alkylpyrrole) with a functional group was found to be soluble in common solvents and water when the substituent bears hydrophilic group with various doping systems such as *p*-dodecylbezene sulfonic acid[19] and camphor sulfonic acid.[20] These polymers not only improve the solubility of PPy, especially in weak polar solvents, but also show high conductivity.

Concurrently, the PPy/clay nanocomposite system, consisting of multilayered silicates and polymer elements, which intercalates between the inter layers of inorganic clay, has been introduced to improve the applicability or physical properties ever since the polymer/clay nanocomposite systems[21] have been introduced in general, such as PPy/montmorillonite nanocomposite synthesized[22] by an emulsion polymerization.[23]

In this study, we synthesized highly soluble PPy via an *in situ* polymerization method, using sodium

Correspondence to: H. J. Choi (hjchoi@inha.ac.kr).
Contract grant sponsor: Korea Science and Engineering Foundation (KOSEF); contract grant number: R17-2007-028-01000-0.

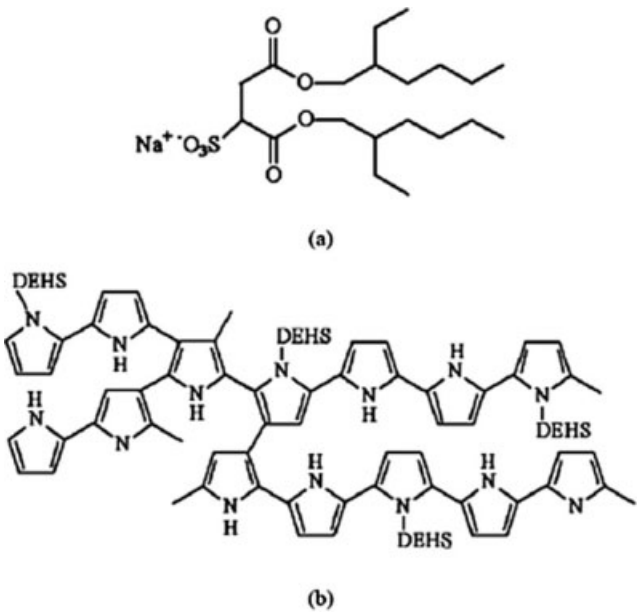

Figure 1 Chemical structure of (a) NaDEHS and (b) PPy.

di-(2-ethylhexyl sulfosuccinate) (NaDEHS) as a dopant, and then prepared PPy-intercalated organoclay nanocomposites using chloroform, for controlling conductivity. After dispersing in silicone oil, it was adopted as an anhydrous ER fluid.

EXPERIMENTAL

The soluble PPy was synthesized by *in situ* doping method with NaDEHS as a dopant [Fig. 1(a)]. At first, both pyrrole (0.4 mol) and $Na^+(DEHS)^-$ (0.2 mol) were dissolved in distilled water at 0°C, and then ammonium peroxydisulfate solution (APS) (0.1 mol) was dissolved in 100 mL distilled water separately. Maintaining the temperature of pyrrole and NaDEHS dispersion at 0°C, the APS solution was slowly dropped into the solution for 3 min. The polymerization occurred for 24 h at 0°C. After the polymerization reaction, synthesized PPy was filtered and washed 5–6 times with 6 L distilled water, and the resultant black cake from the filtering process was dried in a vacuum oven for 3 days. After drying process, the dark powder was simply milled and sieved with 100-μm sieve.

To prepare the polymer/clay nanocomposite, organoclay (OMMT) (Cloisite 25A, Southern Clay Products, Gonzales, TX) was also swollen in chloroform for 24 h. PPy solution and clay dispersion with 25 wt % of OMMT in the nanocomposite were then mixed together and stirred for 24 h to ensure the complete intercalation of PPy chains into multilayered silicates. It was then filtered and dried for the preparation of soluble PPy/organoclay nanocomposite.[24]

The X-ray diffraction (XRD) peak shifted to a lower angle indicated the increase of *d*-spacing as intercalation of the PPy chain into nanoscaled organoclay layers. Both FTIR and NMR were used to investigate the molecular structure and chemical composition. Using scanning electron microscopy (SEM), morphological characteristics were examined. Transmission electron microscope (TEM) was also used to study morphology and sectional diagram of the nanocomposite. Thermal behavior of the PPy/OMMT nanocomposites was examined via TGA. Electrical conductivities of both PPy and PPy/OMMT nanocomposite were measured to be 4.5×10^{-2} and 2.0×10^{-3} S/cm, respectively, using a four-probe method. The conductivity of the PPy/OMMT nanocomposite was then controlled to be semiconducting (1.1×10^{-8} S/cm) via dedoping using NaOH for the ER application, and ER property of the PPy/organoclay nanocomposite system was measured using a rotational rheometer (Physica MC120, Germany) equipped with a DC high-voltage generator. Measurements were conducted at 25°C using a Couette-type concentric cylindrical geometry.

RESULTS AND DISCUSSION

Structural confirmation of the soluble PPy was performed via both NMR and FTIR. The NMR spectra show that pyrrole monomer contains three characteristic peaks in the whole wave number, such as hydrogen peaks of NH group at 8 ppm and hydrogen peaks of α and β-carbon group in pyrrole ring at 6.3 and 6.7 ppm, whereas the dopant DEHS shows four characteristic peaks, that is, two peaks at 4 and 3 ppm and two other peaks in the region of 1.6–0.6 ppm. These peaks from PPy were also found to be slightly shifted as indicated in Figure 2. Because of the structural difference from pyrrole monomer, NMR diagram of the PPy does not show any peak at 8 and 6.3 ppm. This is due to the fact

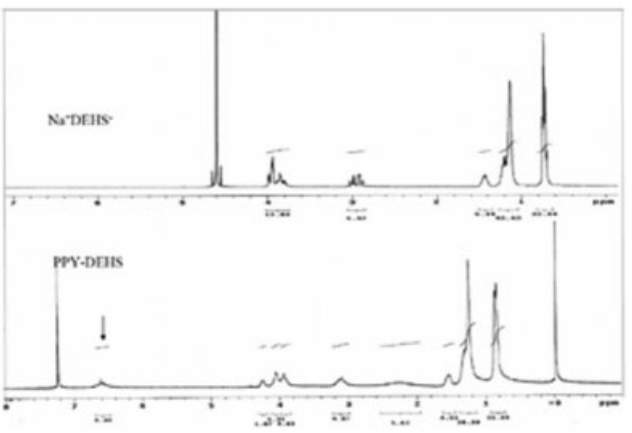

Figure 2 NMR diagram of NaDEHS and PPy.

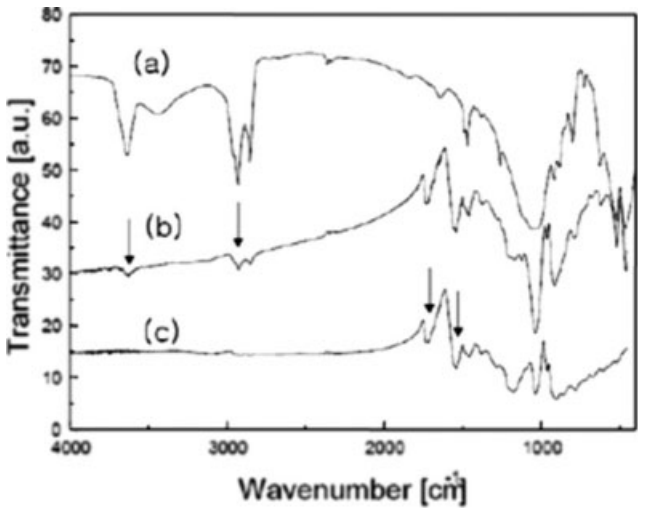

Figure 3 FTIR diagram of (a) OMMT, (b) PPy/OMMT nanocomposite, and (c) PPy.

that the α-carbons in the PPy are linked with other polymer units. In addition, the disappearance of 6.3 ppm peak in this dark black polymer originated from the DEHS group (dopant) contacted with nitrogen in the PPy ring as illustrated in Figure 1(b). Some β-carbons might be linked to other polymer chains, and this is the reason why electrical conductivity of the PPy is higher than other conducting polymers. Minor quantities of hydrogen at β-carbon exist in the polymer chain, showing weak peak at 6.7 ppm. It was found that this NMR analysis could explain the synthetic mechanism of soluble PPy, while confirming that the soluble PPy can be synthesized with DEHS and pyrrole monomer successfully.

Figure 3 represents the FTIR diagram of both soluble PPy and PPy/OMMT nanocomposites. The main peaks of soluble PPy are designated in the range of 500 and 1750 cm^{-1}. As compared with NaDEHS, characteristic peaks of PPy were found at 1550, 900, and 760 cm^{-1}, and these peaks were matched with the results from other groups.[25] In the case of PPy/OMMT nanocomposite, we can observe characteristic peaks at 3640, 2900, and 2840 cm^{-1} representing the existence of OMMT in the composite and 1720, 1530, 1440, and 1370 cm^{-1} for the PPy. From the results of FTIR diagram, we could find that the characteristic peaks of the nanocomposite system from OMMT and PPy are maintained without any significant change of their structural forms.

In addition to FTIR and NMR diagram, TGA also provides the evidence of synthesis of the PPy (Fig. 4). Both PPy and its nanocomposite system exhibit two-step thermal degradation behavior of the first thermal degradation from 280°C and the second weight loss from 360°C, indicating that they were observed to be thermally stable up to 280°C. From the result of thermal degradation, two distinct features, which might be the major characteristics of thermal behavior, could be deduced. The one is the incorporation of dopant on to the backbone chain, and the other is the apparent improvement of thermal stability originated from the nanoscopic dispersion of inorganic clay platelets. The decrease of residual weight in the first step both of PPy and nanocomposite showed similar trend, which is the decomposition of dopant groups. In addition, the starting point of the second step has the same temperature, supporting that the same component would start to decompose in both the systems. With respect to the improved thermal stability, nanocomposites have much higher residual weight at a specific temperature and generate char formation, even though the temperature reached to 300°C. The finally formed char over 820°C is almost 25 wt %, which was original clay content; however, it can be compared with the complete thermal degradation of PPy at 750°C. This kind of retired residual char formation temperature is one of the evidences of the improved thermal stability of the polymer/clay nanocomposite. Usually, the nanoscopic layer spacing, containing the intercalated polymer chains, acts as a thermal barrier to outside heat flow. The supplied heat source forms the char outside of a specific domain, which contains the whole matrix polymer. This wall structure delays the thermal decomposition of inner domain. The continuous heat flow finally converts the overall organic portion in the nanocomposite with the help of inorganic portion.

To examine the ordered internal structure in the nanocomposite, we conducted XRD measurement as shown in Figure 5, showing the shift of peak position from higher value to lower one, which represented the intercalation of PPy chains into the

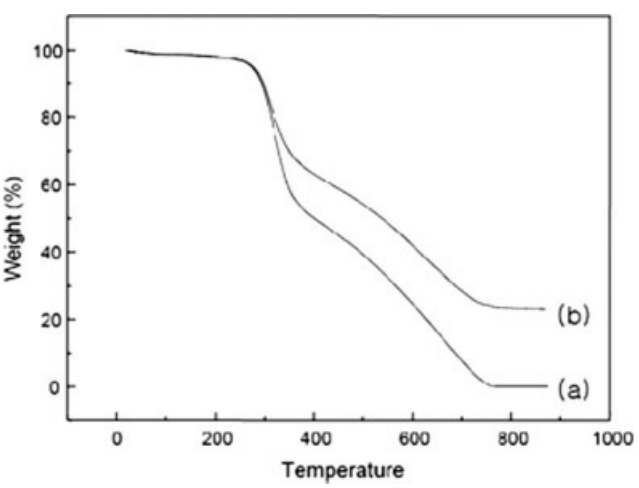

Figure 4 TGA diagram of (a) PPy and (b) PPy/OMMT nanocomposite.

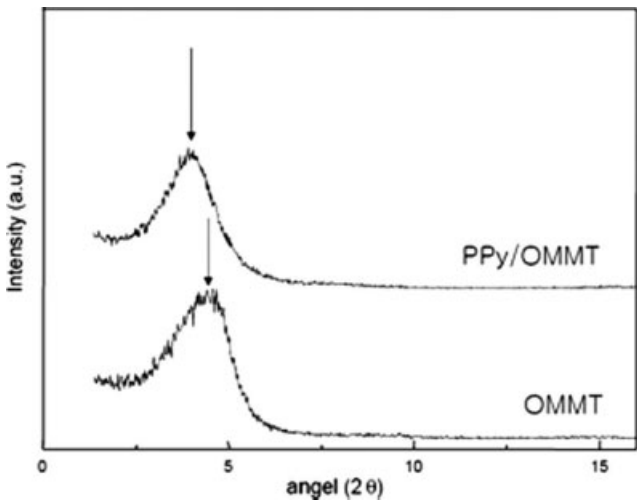

Figure 5 XRD diagram for both OMMT and PPy/OMMT nanocomposites.

interlayer space in nanocomposite. Although the distance between layers of the OMMT was 1.84 nm, the distance between layers of nanocomposite system was estimated to be 2.32 nm, indicating that PPy dissolved well in chloroform and could be intercalated into the clay layers.[26]

Figure 6 shows the SEM micrograph of OMMT(a) and nanocomposite (b) systems, indicating morphological change of the PPy/OMMT nanocomposite. In the nanocomposite systems, we could observe two characteristic morphologies of round shape of PPy and plate-like organoclay particles. This means that the dissolved PPy not only intercalated but also adsorbed on the isolated plate-like clay surfaces. Besides, it was also possible to form the pure PPy particles, which do not interact with clay. In other words, the much different clay surface in pristine clay and nanocomposite can be the evidence of surface adsorption and soluble characteristics of PPy, in addition to the nanoscopic interaction of polymer chain with interlayer structure of layered anticipated.

Figure 7 represents sectional micrograph of the microtomed PPy/OMMT nanocomposite examined by TEM. The clay was found to be well dispersed in PPy from these micrographs in nanoscaled range.

ER properties of the PPy/OMMT-nanocomposite-based ER fluid were examined by using a Couette-type rheometer equipped with DC high-voltage generator. Figure 8 shows both shear stress (a) and shear viscosity of the PPy nanocomposite-based ER fluid (20 wt % particle concentration). The shear stresses were observed to be increased with applied electric strength and showed Bingham fluid behavior, whereas in the high shear rate and no electric field region, the fluid showed pseudo-Newtonian behavior (slope = 0.84). In addition, the shear stress exhibits a plateau region over some shear rate range

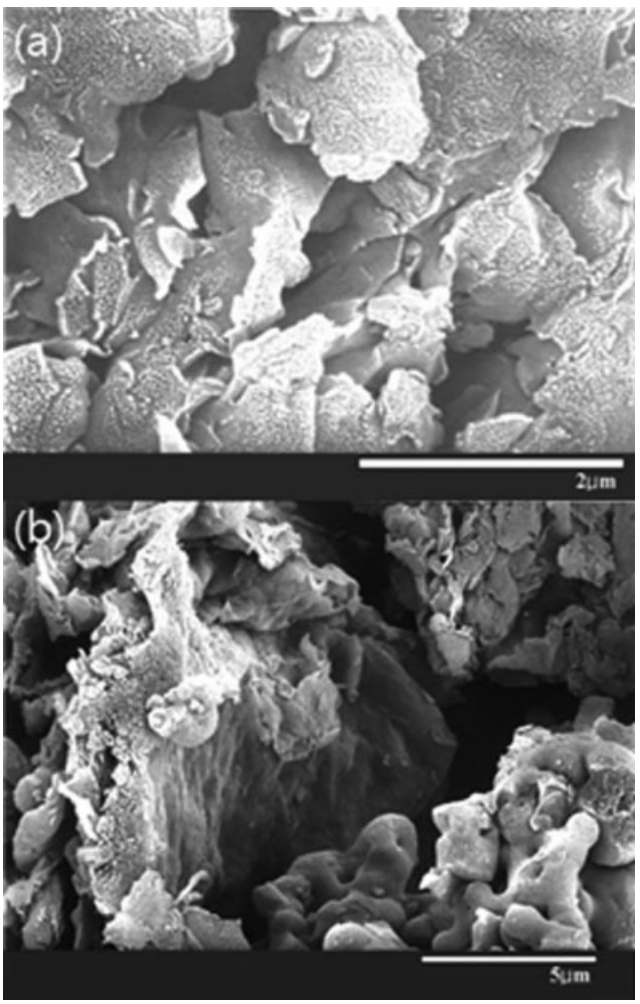

Figure 6 SEM micrograph of (a) OMMT and (b) PPy/OMMT nanocomposite.

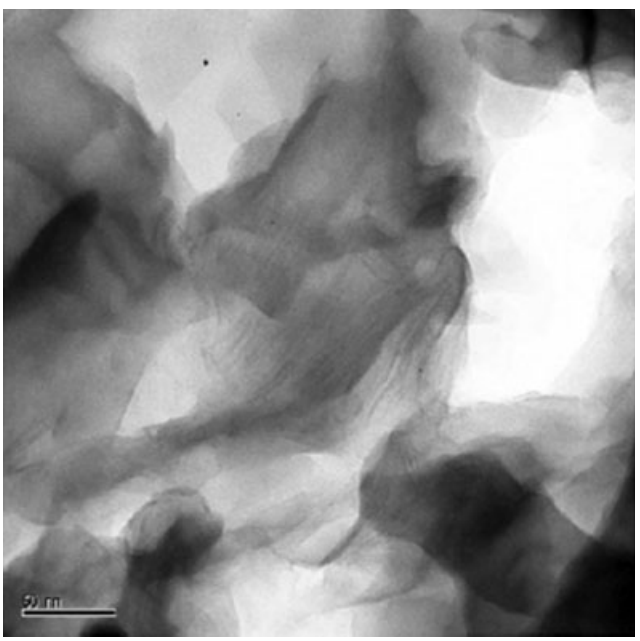

Figure 7 TEM micrograph of PPy/OMMT nanocomposite.

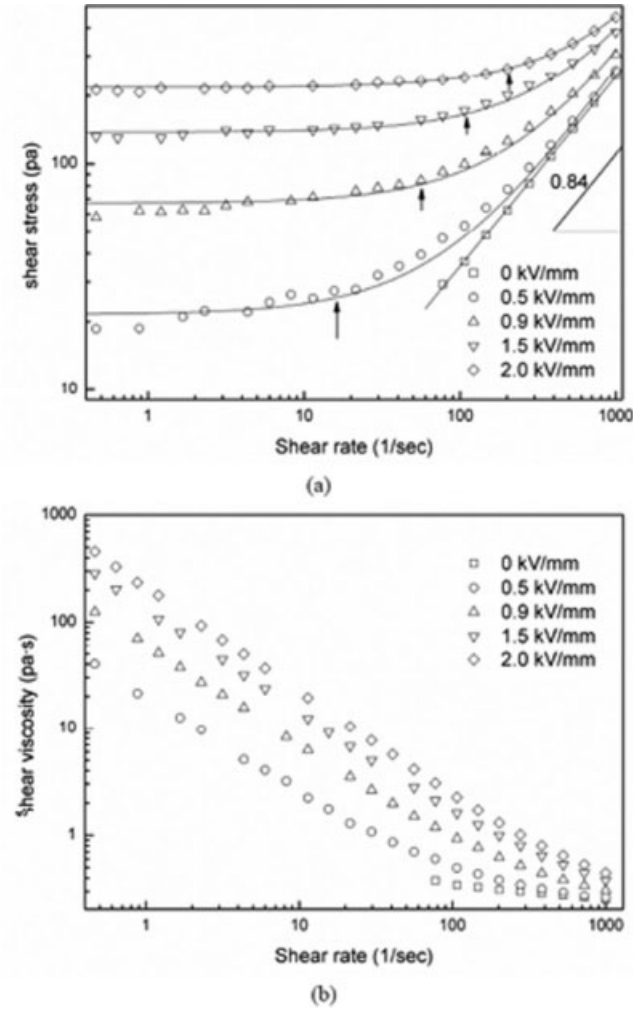

Figure 8 (a) Shear stress versus shear rate (arrow indicates the critical shear rate) and (b) shear viscosity versus shear rate for PPy/OMMT-nanocomposite-based ER fluid under applied electric fields.

under an applied electric field. As the electric fields increase, the plateau shear stress region becomes widen above a critical shear rate indicated as arrows in each electric field. In the low shear rate region, the electrostatic interactions among particles induced by external electric fields are regarded to be dominant when compared with the hydrodynamic interactions induced by the external flow field. The aligned particular chain structures begin to break apart with shear deformation. The broken structures then tend to reform in chains by the applied electric field, depending on the magnitude of the applied shear rate and particle–particle interaction in the fibrils. Interesting behavior of the plateau shear stress (τ) with increasing shear rate up to a critical shear rate ($\dot{\gamma}_{crit}$) has been reported for various ER materials.[27–29] The $\dot{\gamma}_{crit}$ is a transition point of shear rate ($\dot{\gamma}$) at which the fluid begins to exhibit pseudo-Newtonian behavior (τ increases with $\dot{\gamma}$). In this high shear rate range, the particle chains appear to be broken by the shear. Furthermore, there might be no sufficient time for the particles to realign along the electric field direction. In other words, as the shear rate increases, the destruction rate of the fibrils becomes faster than the reformation rate. Finally, in the high shear rate range, the ER fluid shows liquid-like behavior, because the ER chains are fully broken.

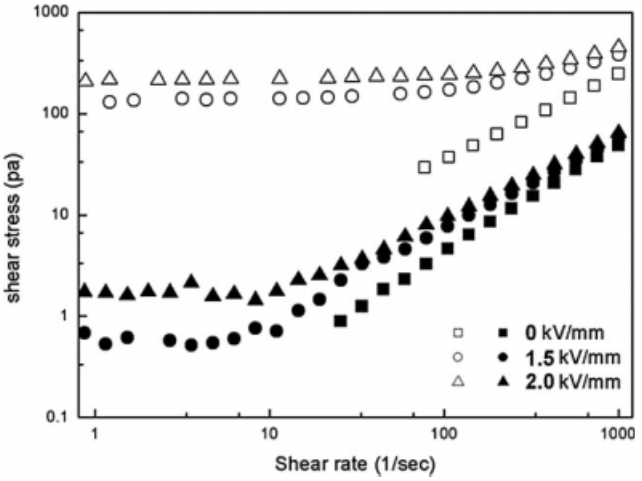

Figure 9 Comparison of shear stress for PPy/OMMT (opened) and PPy/Na^+-MMT (closed) under 0, 1.5, and 2.0 kV/mm.

Furthermore, the ER fluid also shows solid-like behavior at high electric field strength with a residual shear stress, because the chain of ER particles resists the shear. As a result of this aggregated structure, ER fluids under an applied electric field are considered to exhibit Bingham fluid behavior possessing a yield stress (τ_y), which is defined as the shear stress extrapolated from the low shear rate region. The relationship between τ and $\dot{\gamma}$ for the Bingham model is as follows:[30]

$$\tau = \eta\dot{\gamma} + \tau_y \quad (\tau > \tau_y) \qquad (1)$$

$$\dot{\gamma} = 0 \quad (\tau < \tau_y)$$

The fitting of the model equation to the flow curve for PPy/OMMT-nanocomposite-based ER fluids is given in Figure 8(a). The yield stress and the optimal parameters for Bingham model are summarized in Table I.

Furthermore, rheological property of the shear stress of PPy/OMMT-nanocomposite-based ER fluid was compared with that of PPy/Na^+-MMT

TABLE I
Optical parameters in Bingham model equation from the flow curve

	Parameter	0.5 kV/mm	0.9 kV/mm	1.5 kV/mm	2.0 kV/mm
Bingham	τ_y	21.55	67.14	137.8	217.3
	η	0.244	0.25	0.26	0.23

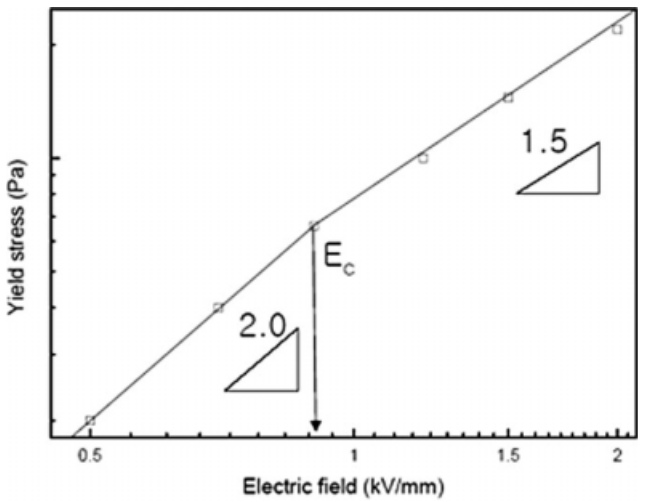

Figure 10 Yield stress of ER fluid as a function of applied electric field with $E_c = 0.9$ kV/mm.

nanocomposite-based ER fluid as shown in Figure 9, in which the PPy/Na^+-MMT was synthesized via an emulsion polymerization method using dodecylbenzenesulfonic acid as both an emulsifier and a dopant.[31] Even though one of the reasons of big difference is due to different particle volume fraction with 10 wt % for PPy/Na^+-MMT-nanocomposite-based ER fluid and 20 wt % for PPy/OMMT-nanocomposite-based ER fluid, the PPy/OMMT-nanocomposite-based ER fluid shows much higher ER performance.

Figure 10 presents the static yield stress, which was estimated from Bingham model, as a function of an applied electric field, showing that the value of α is different from the nonanalytic power law model ($\tau_y = E^{\alpha}$), because nanocomposite particles are not spherical and homogeneous.[32] Furthermore, the critical point of electric field was also found to be 0.9 kV/mm. It can be noted that over the past decades on the ER investigation, yield stress has been interpreted based on either polarization model[33] with $\alpha = 2.0$ or conduction model[34] with $\alpha = 1.5$. However, these models for fitting the data of yield stress as a function of electric field have been regarded to be restricted in a limited range of electric field. Therefore, to represent the yield stress data for a broad range of electric field strengths, Choi et al.[35] proposed the following simple hybrid yield stress formula with the critical electric field strength, E_c to describe the deviation of the yield stress from the polarization model:

$$\tau_y(E_0) = \alpha E_0^2 \left(\frac{\tan h \sqrt{E_0/E_c}}{\sqrt{E_0/E_c}} \right), \tag{2}$$

where the parameter α is known to depend on the dielectric constant of the fluid and particle volume fraction.

Equation (2) clearly possesses the following two asymptotic behaviors at low and high electric field strengths when compared with E_c:

$$\tau_y = \alpha E_0^2 \propto E_0^2, \quad E_0 \ll E_c \tag{3a}$$

$$\tau_y = \alpha \sqrt{E_c} E_0^{3/2} \propto E_0^{3/2}, \quad E_0 \gg E_c \tag{3b}$$

Equation [3(a,b)] shows that τ_y is proportional to E_0^2 at low E_0 and to $E_0^{3/2}$ at high E_0. As represented in Figure 10, we can notice a critical electric field strength from the slope change from the polarization model regime (slope = 2) to the conductivity model regime (slope = 1.5).

Furthermore, to collapse the data into a single curve, we normalized eq. (2) by E_c and τ_y (E_c) = $\alpha E_c^2 \tan h$ (1) = $0.762 \alpha E_c^2$

$$\hat{\tau} = 1.313 \hat{E}^{3/2} \tan h \sqrt{\hat{E}}, \tag{4}$$

where $\hat{E} \equiv E_0/E_c$ and $\hat{\tau} \equiv \tau_y(E_0)/\tau_y(E_c)$. Various ER materials including poly(*p*-phenylene)[36] and mesoporous MCM-41[28] were reported to obey this universal yield stress equation quite well. The experimental data of PPy/OMMT nanocomposite was fully fitted with eq. (4), in which Figure 11 shows the universal scaling curve of the nanocomposite-based ER fluid being collapsed to a single line regardless of the yield stress modes.

CONCLUSION

Soluble PPy was synthesized using a secondary dopant (NaDEHS), and then PPy/OMMT nanocomposite was prepared via a solvent-casting method. The increased interlayer spacing of the clay in the synthesized nanocomposite was confirmed via XRD, and the structure and morphologies of the synthesized soluble PPy and PPy/OMMT nanocomposite were investigated via NMR, FTIR, SEM, and TEM.

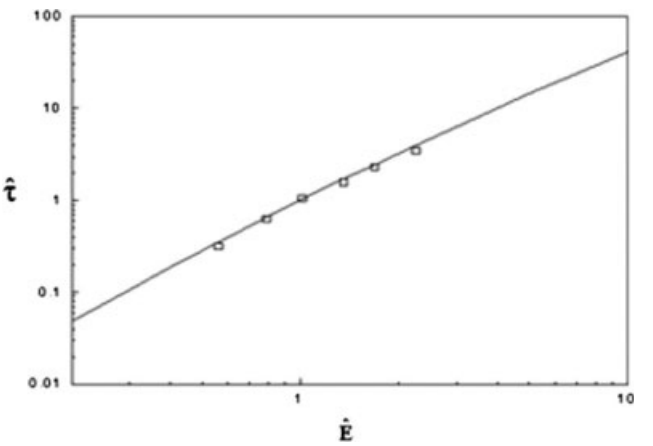

Figure 11 Universal yield stress curve of PPy/OMMT-nanocomposite-based ER fluid.

The particle-suspended ER fluid in silicone oil demonstrated pseudo-Newtonian behavior without an electric field and Bingham plastic behavior under applied electric fields. Yield stress of the nanocomposite increased with applied electric field strength. Universal scaling curve of the nanocomposite-based ER fluid was found to be collapsed into a single line using the critical electric field of 0.9 kV/mm.

References

1. Yoon, D. J.; Kim, Y. D. J Colloid Interface Sci 2006, 303, 573.
2. Zhao, X. P.; Yin, J. B. J Ind Eng Chem 2006, 12, 184.
3. Quadrat, O.; Stejskal, J. J Ind Eng Chem 2006, 12, 352.
4. Lengalova, A.; Pavlinek, V.; Saha, P.; Stejskal, J.; Kitano, T.; Quadrat, O. Phys A 2003, 321, 411.
5. Hiamtup, P.; Sirivat, A.; Jamieson, A. M. J Colloid Interface Sci 2006, 295, 270.
6. Yilmaz, H.; Unal, H. I.; Sari, B. J Appl Polym Sci 2007, 103, 1058.
7. Fang, F. F.; Park, B. J.; Choi, H. J.; Ahn, W. S. Int J Mod Phys B 2007, 21, 4981.
8. Negita, K.; Itou, H. J Colloid Interface Sci 1999, 209, 251.
9. Lee, Y. H.; Kim, C. A.; Jang, W. H.; Choi, H. J.; Jhon, M. S. Polymer 2001, 42, 8277.
10. Fang, F. F.; Choi, H. J.; Joo, J. J Nanosci Nanotech 2008, 8, 1559.
11. Ko, Y. G.; Choi, U. S. J Appl Polym Sci 2006, 102, 4937.
12. Gao, Z.; Zhao, X. P. Polymer 2004, 45, 1609.
13. Kim, S. G.; Choi, H. J.; Jhon, M. S. Macromol Chem Phys 2001, 202, 521.
14. Yoshimoto, S. Macromol Rapid Commun 2005, 26, 857.
15. Kim, J. W.; Kim, S. G.; Choi, H. J.; Jhon, M. S. Macromol Rapid Commun 1999, 20, 450.
16. Yan, H.; Liao, Z. J.; Zhu, X.; Wang, X. M.; Chen, Y.; Zhang, B.; Chen, S. L.; Za, Z. Y. J Appl Polym Sci 2008, 107, 1960.
17. Kim, Y. D.; Song, I. C. J Mater Sci 2002, 37, 5051.
18. Joo, J.; Lee, J. K.; Baeck, J. S.; Kim, K. H.; Oh, E. J.; Epstein, J. Synth Met 2001, 117, 45.
19. Lindfors, T.; Bobacka, J.; Lewenstam, A.; Ivaska, A. Electrochim Acta 1998, 43, 3503.
20. Shen, Y.; Wan, M. Synth Met 1998, 96, 127.
21. Ray, S. S. J Ind Eng Chem 2006, 12, 811.
22. Kim, J. W.; Liu, F.; Choi, H. J.; Hong, S. H.; Joo, J. Polymer 2003, 44, 289.
23. Faquy, P. W.; Lucas, R. A.; Ma, W. Colloids Surf 1995, 105, 105.
24. Park, D. P.; Sung, J. H.; Lim, S. T.; Choi, H. J.; Jhon, M. S. J Mater Sci Lett 2003, 22, 1299.
25. Rasika Dias, H. V.; Fianchini, M.; Gamini Rajapakse, G. Polymer 2006, 47, 7349.
26. Kim, B. H.; Jung, J. H.; Hong, S. H.; Joo, J.; Epstein, A. J.; Mizoguchi, K.; Kim, J. W.; Choi, H. J. Macromolecules 2002, 35, 1419.
27. Hong, C. H.; Choi, H. J.; Jhon, M. S. Chem Mater 2006, 18, 2771.
28. Cheng, Q.; Pavlinek, V.; Lengalova, A.; Li, C.; Belza, T.; Saha, P. Microporous Mesoporous Mater 2006, 94, 193.
29. Cho, M. S.; Cho, Y. H.; Choi, H. J.; Jhon, M. S. Langmuir 2003, 19, 5875.
30. See, H. J Ind Eng Chem 2004, 10, 1132.
31. Kim, B. H.; Hong, S. H.; Joo, J.; Park, L. W.; Epstein, A. J.; Kim, J. W.; Choi, H. J. J Appl Phys 2004, 95, 2697.
32. Kim, D. H.; Kim, Y. D. J Ind Eng Chem 2007, 13, 879.
33. Block, H.; Kelly, J. P. J Phys D: Appl Phys 1988, 21, 1661.
34. Davis, L. C. J Appl Phys 1997, 81, 1985.
35. Choi, H. J.; Cho, M. S.; Kim, J. W.; Kim, C. A.; Jhon, M. S. Appl Phys Lett 2001, 78, 3806.
36. Sim, I. S.; Kim, J. W.; Choi, H. J.; Kim, C. A.; Jhon, M. S. Chem Mater 2001, 13, 1243.